

1 **Revision 1** correction date: July the 15th 2013

2 **North-American microtektites are more oxidized than tektites.**

3

4 Gabriele Giuli¹, Maria Rita Cicconi¹, Sigrid Griet Eeckhout^{2,*}, Christian Koeberl³,

5 Billy P. Glass⁴, Giovanni Pratesi⁵, Mariangela Cestelli-Guidi⁶ and Eleonora Paris¹.

6

7 ¹School of Science and Technology, Geology Division, University of Camerino, Italy;

8 gabriele.giuli@unicam.it.

9 ²European Synchrotron Radiation Facility (ESRF), Grenoble, France.

10 ³Department of Lithospheric Research, University of Vienna, Althanstrasse 14, A-

11 1090 Vienna, Austria; *and* Natural History Museum, Burgring 7, A-1010 Vienna,

12 Austria.

13 ⁴Department of Geological Sciences, University of Delaware, Newark, DE 19716,

14 USA.

15 ⁵Dipartimento di Scienze della Terra, Università di Firenze, Italy

16 ⁶Laboratori Nazionali Frascati, Istituto Nazionale Fisica Nucleare, Via Enrico Fermi,
17 Frascati, I.

18

19 **Running title:** Fe oxidation state in microtektites

20

21 **Corresponding author:** Gabriele Giuli e-mail: gabriele.giuli@unicam.it

22

23 * Present address: ESV EURIDICE GIE, Mol, Belgium.

24

25 **Abstract**

26

27 Iron oxidation states and coordination numbers have been determined by micro-
28 X-ray Absorption Near Edge Spectroscopy (XANES) on the cores of a large group of
29 microtektites from the Australasian, Ivory Coast, and North American (NA) tektite
30 strewn fields. The North American microtektites used in this study have been
31 collected from five sites at different distances from the source crater; most have SiO₂
32 content between 70 and 80 wt%. Accurate analysis of the pre-edge peak energy
33 position and integrated area allowed determination of Fe³⁺/(Fe²⁺+Fe³⁺) ratios on all
34 samples with an estimated error of ±0.05.

35 Microtektites from the Australasian and Ivory Coast strewn fields show low
36 values of the Fe³⁺/(Fe²⁺+Fe³⁺) ratios, in fair agreement with tektites from the same
37 strewn field. In contrast, microtektites from the North American strewn fields show a
38 wide range of Fe³⁺/(Fe²⁺+Fe³⁺) ratios from 0.02 to ca. 0.61. Comparison of Fe
39 oxidation state data with chemical composition do not show any relation between
40 Fe³⁺/(Fe²⁺+Fe³⁺) ratios and Na, Ca, or K contents, thus suggesting that the high Fe
41 oxidation states are not the consequence of sea-water alteration.

42 The difference between the Fe oxidation state of tektites and microtektites from
43 the North American strewn fields suggests that some factors in the formation of the
44 North American microtektites were different than for the North American tektites and
45 for microtektites in the other strewn fields.

46 Previous Fe oxidation state data on NA tektites strongly suggest that the wide
47 range in Fe oxidation state we found on NA microtektites is not related to lateral
48 heterogeneity of the target rocks. Despite a correlation between microtektite oxidation
49 state and distance from the source crater, we maintain that Fe oxidation state is not
50 related only to the microtektite droplet flight distance. This is in keeping with the fact
51 that no significant variations in the Fe oxidation state have been found in

52 microtektites from the Australasian strewn field, even for Australasian microtektites
53 recovered in Antarctica. The Fe oxidation state in North American microtektites could
54 be explained by interaction of melt droplets with a H₂O-rich vapor plumes generated
55 during the impact. These data point out that some difference must exist between the
56 thermal histories of microtektites and tektites from the NA strewn field. Moreover,
57 microtektites from the NA strewn field show also distinctively higher oxidation states
58 than those from Ivory Coast or the Australasian strewn fields.

59

60 **Keywords:** impact glasses, tektites, microtektites, Fe local structure, XANES

61

62

INTRODUCTION

63 Microtektites are small (<1 mm) splash-form impact glasses related to tektites,
64 which are found scattered over regions of the Earth's surface called strewn fields (e.g.
65 Koeberl, 1986, 1994). They are associated with three of the four tektite strewn fields
66 so far known: the North American (NA), the Ivory Coast, and the Australasian strewn
67 fields. They are generally found in deep sea cores (e.g., Glass, 1967, 1968, 1972;
68 Cassidy et al., 1969), and their distribution greatly contributed to establish the limits
69 of tektites strewn fields (see Glass, 1990; Glass and Pizzuto, 1994).

70 Despite the availability of geochemical studies on microtektites (see Glass et al,
71 2004 and references therein), few studies exist of the Fe coordination number and
72 oxidation state in such materials (Senftle et al., 1969). As microtektites constitute a
73 large fraction of the mass of the glass produced by a tektite-generating impact event,
74 such studies are of great importance for a more complete understanding of impact-
75 generated glasses and, in particular, to try reconstructing the oxygen fugacity
76 conditions prevailing during impact melt formation.

77 Previous data have shown a set of microtektites from the North American strewn
78 field (collected at the DSDP Site 94) to be consistently more oxidized with respect to
79 microtektites from the other strewn fields (Giuli et al., 2008b). Moreover, another
80 study of macroscopic tektites from the North-American strewn fields showed no
81 variation of the Fe oxidation state as a function of tektite provenance and composition
82 (Giuli et al., 2010a), thus confirming that the strong variation in the Fe oxidation state
83 previously found in NA microtektites does not depend on lateral heterogeneities of
84 the target rock.

85 This case is unique among tektites and microtektites and, if confirmed, may
86 contribute to a better understanding of microtektite formation processes. To expand
87 on our previous data, we studied a larger set of microtektites from the North
88 American strewn field collected from three additional cores (RC9-58 and DSDP sites
89 612 and 149) and from Barbados. These samples have been collected at different
90 distances from the source crater and span a wider compositional range than those
91 previously analyzed. The use of a small X-ray beam allowed to probe the core of the
92 studied samples, thus avoiding possible alteration rims.

93

94

SAMPLES AND EXPERIMENTAL

95 Microtektite samples consist of glassy spherules retrieved from deep-sea cores
96 from three different strewn fields: Australasian microtektites (including 1 normal, 3
97 high Ni, 1 high Mg, and 1 intermediate sample) have been sampled from ODP Site
98 769A, and cores RC12-331 and RC14-46; Ivory Coast microtektites (10 samples)
99 come from core K9-56; North American microtektites (25 samples) come from DSDP
100 Sites 612, 94, and 149, core RC9-58, and from Bath Cliff, Barbados. The
101 compositions of these samples have already been studied (Glass et al., 2004) and are

102 reported in Table 1. The spherules have been embedded in resin, ground down to
103 expose an interior surface, and polished. Typical dimensions range from 400 to 800
104 μm diameter. Both scanning electron microscopy and optical microscopy indicate that
105 no crystals are present. As shown in Fig. 1, most of the microtektite samples display
106 silica contents ranging between ca. 70 and 80 wt % and alkali contents ranging
107 between ca. 3 and 5 wt %.

108 The standards used for X-ray absorption near edge spectroscopy (XANES)
109 measurements are: a staurolite from Canton Ticino (Switzerland) and a synthetic Fe-
110 akermanite for Fe^{2+} in tetrahedral coordination; a grandidierite from Madagascar for
111 Fe^{2+} in trigonal bipyramidal coordination; a synthetic kirschsteinite, a synthetic
112 orthopyroxene ($\text{En}_{60}\text{Fs}_{40}$) and a siderite from Erzberg (Austria) for Fe^{2+} in octahedral
113 coordination; an andradite from Italy, and an aegirine from Malawi for Fe^{3+} in
114 octahedral coordination; a yoderite from Mautia Hills (Tanzania) for Fe^{3+} in 5-fold
115 coordination; a tetra-ferriphlogopite from Tapira (Brasil) for Fe^{3+} in 4-fold
116 coordination (Giuli et al., 2001). The natural standards were separated by hand-
117 picking from cm-sized crystals choosing the clearest portions to avoid impurities. All
118 the standards were checked for purity by both optical microscopy and X-ray
119 diffraction. Model compounds for X-ray Absorption Spectroscopy (XAS)
120 measurement were prepared by smearing finely ground powder on a kapton tape,
121 whereas the glass samples were prepared as slides with polished surfaces. Fe K-edge
122 XANES spectra were recorded at room temperature at the ESRF (European
123 Synchrotron Radiation Facility) storage ring on the undulator beamline ID26
124 (Gauthier et al., 1999; Solé et al., 1999) operating at 6 GeV. A Si(311) double-crystal
125 monochromator was used, providing an energy resolution of ~ 0.2 eV at the Fe K-
126 edge. However, the main limitation for energy resolution is the finite core-hole width

127 of the absorbing element (~ 1.15 eV at the Fe K-edge, Krause and Oliver 1979),
128 resulting in a convoluted energy resolution of ~ 1.4 eV. The energy was calibrated by
129 defining the first derivative peak of a metallic Fe reference foil to be at 7112.0 eV.
130 Two Si mirrors were used for the harmonics rejection of the incident X-ray beam.
131 Beam dimension at the sample was 55x120 micrometers. For each sample the beam
132 has been carefully centered by means of vertical and horizontal scans so as to allow
133 probing the inner part of the spherules far from the border, thus avoiding possible
134 alteration rims. XANES data were recorded in quick-scan mode by simultaneously
135 scanning the monochromator angle and the undulator gap with a typical energy step
136 of 0.1 eV and counting 44 ms per point. Each scan took 120 seconds and an average
137 of 12 spectra was taken per sample. The spectra were acquired in fluorescence mode,
138 using a Si photo-diode, and I_0 was monitored by measuring the fluorescence signal of
139 a titanium foil using a Si photo-diode. The flat surface of the sample was positioned at
140 45° with respect to the beam and the detector. Average of about 12 scans for each
141 sample allowed us to obtain very good signal to noise ratios despite the small beam
142 size. The energy reproducibility has been estimated to be ± 0.03 eV or better.

143 Experimental XANES spectra were reduced by background subtraction with a
144 linear function and then normalized for atomic absorption on the average absorption
145 coefficient of the spectral region from 7170 to 7350 eV. The threshold energy was
146 taken as the first maximum of the first derivative of the spectra, whereas peak
147 positions were obtained by calculating the second derivative of the spectra. Pre-edge
148 peak analysis was carried out following the same procedure reported in Wilke et al.
149 (2001) and Giuli et al. (2002). The pre-edge peak was fitted by a sum of pseudo-Voigt
150 functions, and their intensities along with energy positions were compared with those
151 of the standards analysed here and others from the literature (e.g., Wilke et al., 2001;

152 Farges, 2001) in order to extract information on Fe oxidation state and coordination
153 number in these microtektites. Particular care was taken in using the smallest possible
154 number of components in the pre-edge peak fitting procedure. In particular, the
155 number (and, in some cases, the approximate energy) of the components was
156 constrained to equal the number (and approximate energy) of the minima in the
157 second derivative spectrum of the pre-edge peak. Several different procedures have
158 been attempted for peak fitting: simultaneous fitting of the background and the
159 pseudo-Voigt component; preliminary background subtraction followed by fitting
160 with pseudo-Voigt component allowing the components to have different full width at
161 half maximum (FWHM) or Lorentian character; preliminary background subtraction
162 followed by fitting with pseudo-Voigt component constrained to have the same
163 FWHM and Lorentian character. This last procedure has been shown to produce the
164 best results in terms of data scatter.

165 The precision of the fitted pre-edge peak centroid energy and integrated area are
166 ± 0.02 eV and ± 0.015 , respectively. Mixing lines have been calculated as linear
167 combination of two pre-edge peaks representative of Fe²⁺ and Fe³⁺ (see Giuli et al.,
168 2003, 2011). We tried different integrated areas for Fe²⁺ and Fe³⁺ until a calculated
169 mixing line was found to match the integrated area and centroid energy of a set of
170 glasses; then it has been used to evaluate the contribution of the divalent and trivalent
171 Fe to the experimentally measured pre-edge peaks. This procedure implies that a
172 single spectrum (pre-edge peak integrated area and centroid energy) does not allow an
173 accurate determination of the Fe³⁺/(Fe²⁺+Fe³⁺) ratio unless constraints are applied on
174 the integrated areas relative to the Fe³⁺ and Fe²⁺ species contributing to that spectrum.
175 This procedure, applied to a set of synthetic glasses (Giuli et al., 2011), resulted in
176 accurate determinations of Fe³⁺/(Fe²⁺+Fe³⁺) ratios that are in agreement with

177 independent titration data within ± 0.03 . In the present case we estimate the error in
178 the determination of $\text{Fe}^{3+}/(\text{Fe}^{2+}+\text{Fe}^{3+})$ ratios on microtektite samples to be ± 0.05

179

180

XANES RESULTS

181 Examples of experimental Fe K-edge XANES spectra are shown in Fig. 2 for five
182 groups of microtektites: Australasian and Ivory Coast in Fig. 2a and 2b, respectively,
183 and three groups of North American microtektites in Fig. 2 c, d, and e. The shape and
184 edge energy position of the Australasian and Ivory Coast microtektite spectra are very
185 similar to those of splash form tektites studied previously (Giuli et al., 2002),
186 suggesting the presence of predominantly divalent Fe. On the other hand, the spectra
187 of the North American microtektite samples display significant differences in both the
188 shape of the XANES spectra and their first derivative that are clearly related to
189 variations in the Fe oxidation state. Moreover, also significant changes in the pre-edge
190 peak (labeled P) are visible.

191 The pre-edge peak is related to an *s-d* like electronic transition and, despite being
192 dipole-forbidden, can become partially allowed by mixing of the *d*-states of the
193 transition metal with the *p*-states of the surrounding oxygen atoms. This means that
194 the pre-edge peak energy position and intensity depend strongly on both the geometry
195 around Fe and on the mean Fe oxidation state (Calas and Petiau, 1983; Brown et al.,
196 1995). As already shown in the literature, accurate evaluation of the pre-edge peak
197 centroid energy and integrated area and comparison with those of Fe model
198 compounds can provide quantitative information on both Fe oxidation state and
199 coordination environment (see Calas and Petiau, 1983; Brown et al., 1995; Wilke et
200 al., 2001, 2006; Farges, 2001; Giuli et al., 2002, 2011): its intensity will be almost

201 zero in case of regular octahedral symmetry (O_h) around the absorber, whereas it will
202 reach its maximum in the case of tetrahedral symmetry (T_d).

203 The background subtracted pre-edge peaks of the microtektite XANES spectra are
204 shown in Fig. 3 (a-e), along with the pseudo-Voigt components used in the fitting
205 procedure and their sums, whereas their centroid energies and integrated areas are
206 reported in Table 2. Each pre-edge peak can be fitted with two to three components
207 whose energies (ca. 7112.6, 7113.9-7114.3, and 7114.5-7115.3 eV) are consistent
208 with those of divalent and trivalent Fe model compounds. In particular, while the first
209 and last components can be ascribed to contributions from Fe^{2+} and Fe^{3+} respectively,
210 the component at intermediate energy results from contributions by both Fe^{2+} and
211 Fe^{3+} . The relative importance of divalent or trivalent Fe causes an increase of the
212 respective components resulting in an energy shift of the pre-edge peak centroid.

213 The integrated area of the pre-edge peaks vs. their centroid energies are plotted in
214 Figure 4 (a,b) along with the data of Fe model compounds analysed here and by
215 others (Wilke et al., 2001; Farges, 2001; Giuli et al., 2002). For the sake of simplicity,
216 the relative energy is plotted (0 refers to the first maximum of the first derivative of
217 metallic Fe spectrum) in order to avoid confusion when comparing data with literature
218 data where a different energy value of metallic Fe has been chosen. All divalent Fe
219 model compounds plot at energies close to 0.9 eV above the metallic Fe edge,
220 whereas trivalent Fe model compounds plot at energies close to 2.4 eV. At constant
221 energy, the intensity of the model compounds pre-edge peaks varies according to the
222 Fe coordination geometry (the shaded ellipses refer to the range of coordination
223 numbers in Fe model compounds).

224 The Australasian and Ivory Coast microtektites data (Fig. 4a) plot within a narrow
225 region close in energy to that of divalent Fe model compounds, meaning that most of

226 the Fe is divalent. Three mixing lines (dotted line with small diamonds) have been
227 calculated by a linear combination of:

228 i) a pre-edge peak with a centroid at 0.9 eV above the edge of metallic iron and an
229 integrated area intermediate to that of $^{[4]}\text{Fe}^{2+}$ and $^{[5]}\text{Fe}^{2+}$ model compounds;

230 ii) a pre-edge peak with a centroid at 2.4 eV above the edge of metallic iron and
231 integrated area typical of $^{[4]}\text{Fe}^{3+}$, or $^{[5]}\text{Fe}^{3+}$, or $^{[6]}\text{Fe}^{3+}$.

232 These mixing lines stem from a region with intermediate intensity between $^{[4]}\text{Fe}^{2+}$
233 and $^{[5]}\text{Fe}^{2+}$ thus meaning that the divalent Fe in these glasses is present both in [4] and
234 [5] coordination. Should $^{[6]}\text{Fe}^{2+}$ be present in consistent amounts it would drastically
235 lower the pre-edge peak intensity. However, its presence in minor amounts cannot be
236 ruled out by XANES data alone. The two mixing lines that best fit the experimental
237 points are those calculated using $^{[4]}\text{Fe}^{3+}$ and $^{[5]}\text{Fe}^{3+}$ pre-edge peak intensity; this
238 suggests that trivalent iron may be in [4] and [5] coordination.

239 Comparison between the experimental pre-edge peak data and the calculated
240 mixing lines provided quantitative $\text{Fe}^{3+}/(\text{Fe}^{3+}+\text{Fe}^{2+})$ ratios $\leq 0.1 \pm 0.05$ for most of the
241 samples and up to 0.21 for four samples (0.13, 0.15, 0.19, and 0.21). Based on the
242 precision of the energy (± 0.03 and ± 0.05 eV for the Ivory Coast and Australasian
243 spectra respectively), we estimate the error in the $\text{Fe}^{3+}/(\text{Fe}^{3+} + \text{Fe}^{2+})$ ratios to be within
244 ± 0.05 . These results are in keeping with known Fe oxidation states of Australasian
245 and Ivory Coast microtektites.

246 On the other hand, North American microtektites display centroid energy values
247 much higher than those of the Australasian and Ivory Coast microtektites, indicating
248 significantly higher contributions from trivalent Fe (Fig. 4b). Three mixing lines have
249 been calculated as in the previous case. It is worth remarking that this set of mixing
250 lines originates from a point with the average intensity of a wide set of tektites

251 analysed so far (Giuli et al., 2002, 2010a, 2010b). As in the Ivory Coast and
252 Australasian microtektite case, the average coordination number of divalent Fe is
253 intermediate between [4] and [5]. However, while many the samples can be explained
254 as consisting of a mixture of $^{[4]}\text{Fe}^{2+}$, $^{[5]}\text{Fe}^{2+}$, $^{[4]}\text{Fe}^{3+}$, $^{[5]}\text{Fe}^{3+}$, (see Calas et al., 1983;
255 Brown et al., 1995; Rossano et al., 2009; Wilke et al., 2004, 2006; Jackson et al.,
256 2005; Giuli et al., 2002, 2011; Weigel et al., 2006, 2008), which are common Fe
257 species usually found in silicate melts and glasses, the microtektites from Barbados
258 have distinctly lower integrated areas, compatible with the presence of $^{[6]}\text{Fe}^{3+}$ along
259 with other Fe species. Despite this Fe species not being very common in silicate melts
260 and glasses, it has been observed by Wilke et al. (2004) in synthetic glasses of basaltic
261 composition. Comparison between the experimental pre-edge peak data of NA
262 microtektites and the calculated mixing lines provided quantitative $\text{Fe}^{3+}/(\text{Fe}^{3+}+\text{Fe}^{2+})$
263 ratios ranging from 0.02 and 0.61 ± 0.05 .

264

265

DISCUSSION

266 XANES data have been presented for a large set of microtektites from the
267 Australasian, Ivory Coast and North American strewn fields (6, 10, and 26 samples
268 respectively). Accurate analysis of the pre-edge peak allowed determination of the Fe
269 oxidation state for all the samples analyzed (see Table 2). To the authors' knowledge
270 this is the first report of the Fe oxidation state in such a large set of microtektites.

271 Most of the samples from the Australasian and Ivory Coast strewn fields display
272 values consistent with $\text{Fe}^{3+}/(\text{Fe}^{2+}+\text{Fe}^{3+})$ ratios $\leq 0.1 \pm 0.05$, with only four samples
273 displaying slightly larger values (0.13, 0.15, 0.19, and 0.21). Thus, in these two
274 strewn fields, microtektites display Fe oxidation states and coordination numbers
275 fairly similar to those of macroscopic tektites (Fudali et al., 1987; Dunlap et al, 1998;

276 Rossano et al., 1999; Giuli et al., 2002, 2010a, 2010b). On the other hand,
277 microtektites from the North American strewn field exhibit much higher values of the
278 $\text{Fe}^{3+}/(\text{Fe}^{2+}+\text{Fe}^{3+})$ ratios, from 0.02 up to 0.61 ± 0.05 .

279 As there is the possibility that a long residence time in marine sediments may have
280 altered the microtektite glasses, we checked whether some correlation may exist
281 between Fe oxidation state and chemical composition which may be indicative of sea-
282 water alteration induced oxidation (see Giorgetti et al., 2001; Alt and Mata, 2000). In
283 Fig. 5 the alkali content is plotted as a function of the $\text{Fe}^{3+}/(\text{Fe}^{2+}+\text{Fe}^{3+})$ ratio of all the
284 microtektites analyzed here. No obvious correlation has been found between Fe
285 oxidation state and chemical composition of the studied microtektites. In particular,
286 no inverse relationship has been found with the Na content, which might have been
287 expected in case of oxidation due to sea-water alteration, nor any other correlation has
288 been found that would suggest alteration in a marine environment. Moreover, a tektite
289 fragment retrieved along with microtektites from a core in the DSDP Site 612 (and
290 which, thus, should have similar degree of alteration) displayed an $\text{Fe}^{3+}/(\text{Fe}^{2+}+\text{Fe}^{3+})$
291 ratio of 0.05 ± 0.05 (Giuli et al., 2010a), consistent with values for the tektites found
292 on land, thus further suggesting that there was no alteration-induced oxidation in these
293 microtektite samples. Also preliminary micro-infrared spectroscopy data on a few
294 microtektite samples (see supplementary material) yielded low water contents in the
295 range between 35 to 455 ppm, similar to those of NA tektites (see Beran and Koeberl,
296 1997; Giuli et al., 2010c (IMA abstract)), reinforcing the suggestion that the
297 microtektites analyzed here did not suffer alteration.

298 Thus, we believe that the oxidation states determined are a signature of the
299 formation process of these NA microtektites, and not the product of subsequent
300 alteration in the sediment. Interestingly, pre-edge data of all NA microtektites seem to

301 define different trends all originating from a single narrow region whose energy and
302 intensity is typical of most splash form tektites studied so far. Also, previous data on
303 NA tektites (Giuli et al., 2010a) from different locations and with different chemistry
304 clearly show that the Fe oxidation state of tektites does not vary according to tektite
305 composition. This indicates that the wide range of Fe oxidation states we found in NA
306 microtektites is not related to lateral heterogeneity of the target rock.

307 A possible explanation may involve formation of microtektites with Fe oxidation
308 state and coordination number similar to that of tektites and Trinity glass (a glass
309 formed by high temperature melting of desert sand during the first atomic bomb test
310 at the Trinity site; see Glass et al., 1988; Giuli et al., 2010b), and subsequent
311 oxidation when still molten.

312 Although a similarity with impact glass spherules from the K/T boundary, which
313 showed a similar trend in pre-edge peak data extending up to 100% trivalent Fe, may
314 be envisioned (Giuli et al., 2005, 2008a), no clear explanation can be provided yet for
315 the high Fe oxidation state of the North American microtektites.

316 In this respect it is interesting to notice that the Fe oxidation state of the studied
317 microtektites seems to increase with the distance of the collection site from the source
318 crater. In Fig. 6 the fraction of the trivalent Fe is shown as a function of the distance
319 of the microtektite collection site from the Chesapeake Bay impact structure: even
320 though microtektites within every collection site display a range of Fe oxidation
321 states, it is evident that the fraction of trivalent Fe tends to increase with the distance
322 from the crater. Although it would be tempting to relate the increase of the trivalent
323 Fe fraction to the oxidation of melt in air during the travel from the source crater to
324 the landing site, this hypothesis has to be discounted when comparing data for
325 Australasian microtektites with those found in Antarctica (Folco et al., 2010). In fact,

326 recent analyses of the Fe oxidation state on 29 Antarctic microtektite samples (Giuli
327 et al., 2012) showed that the fraction of trivalent Fe is lower than 0.1, thus being
328 compatible with the Fe oxidation state of Australasian tektites previously analyzed
329 (see Dunlap et al. 1998; Dunlap and Sibley, 2004; Rossano et al., 1999; Giuli et al.,
330 2002) and the microtektites analyzed here. In that case, a flight distance of up to ca.
331 11000 km from the putative location of the source crater did not produce any
332 noticeable oxidation of the Fe in the microtektite melt droplet; thus, oxidation in air
333 during the flight is unlikely to be responsible for the higher Fe oxidation state of NA
334 microtektites compared to tektites.

335

336

IMPLICATIONS

337 Even though the Fe oxidation in North American microtektites could be explained
338 by interaction of melt droplets with a H₂O-rich vapor plumes generated during the
339 impact, no definitive explanation can yet be given for the anomalously high Fe
340 oxidation state of NA microtektites and more studies are needed to understand the
341 factors affecting the Fe oxidation state of these samples. However, the marked
342 difference in the $Fe^{3+}/(Fe^{2+}+Fe^{3+})$ ratio of tektites and microtektites from the North
343 American strewn field raises the question whether or not microtektites should simply
344 be considered as microscopic analogous of tektites or if some difference exists
345 between their formation mechanisms. Furthermore, our results indicate that some
346 differences must exist in the thermal (and/or oxygen fugacity) histories of
347 microtektites from the NA strewn field compared with those from the Ivory Coast or
348 the Australasian strewn fields.

349

350

ACKNOWLEDGMENTS

351 The authors wish to thank the staff of beamline ID-26 (ESRF, F) for kind assistance
352 during the experiment. Helpful comments by the reviewers are also greatly
353 appreciated.

354

355 **REFERENCES**

- 356 Alt, C.J., and Mata B.P. (2000) On the role of microbes in the alteration of submarine
357 basaltic glass: a TEM study. *Earth And Planetary Science Letters*, **181**, 301-
358 313.
- 359 Brown, G.E., Farges, F., and Calas, G. (1995) X-ray scattering and X-ray
360 spectroscopy studies of silicate melts. In *Structure, dynamics and properties of*
361 *silicate melts* (J.F. Stebbins, P.F. McMillan, D.B. Dingwell, eds.) Review in
362 *Mineralogy* 32, 317-410.
- 363 Burns, C.A. (1985) A study of North American microtektites from Barbados, West
364 Indies: M.S. Thesis, University of Delaware, Newark, Delaware, U.S.A. 120
365 pp.
- 366 Calas, G. and Petiau, J. (1983) Coordination of iron in oxide glasses through high-
367 resolution K-edge spectra: information from the pre-edge. *Solid State*
368 *Communications*, **48**, 625-629.
- 369 Cassidy, W.A., Glass, B.P., and Heezen, B.C. (1969) Physical and chemical
370 properties of Australasian microtektites. *Journal of Geophysical Research* **74**,
371 1008–1025.
- 372 Dunlap, R.A., Eelman, D.A., and MacKay, G.R. (1998) A Mössbauer effect
373 investigation of correlated hyperfine parameters in natural glasses (tektites).
374 *Journal of Non-Crystalline Solids*, **223**, 141-146.
- 375 Dunlap, R.A. and Sibley, A.D.E. (2004) A Mössbauer effect study of Fe site
376 occupancies in Australasian tektites. *Journal of Non-Crystalline Solids* **337**,
377 36-41.

- 378 Farges, F. (2001) Crystal-chemistry of Fe in natural grandidierites: a XAFS
379 spectroscopy study at the Fe K-edge. *Physics and Chemistry of Minerals*, **28**,
380 619-629.
- 381 Folco, L, Glass, B.P., D’Orazio, M., and Rochette, P. (2010) A common volatilization
382 trend in Transantarctic Mountain and Australasian microtektites: Implications
383 for their formation model and parent crater location. *Earth and Planetary
384 Science Letters*, **293**, 135-139.
- 385 Fudali, R.F., Dyar, M.D., Griscom, D.L., and Schreiber, D. (1987) The oxidation state
386 of iron in tektite glass. *Geochimica et Cosmochimica Acta*, **51**, 2749-2756.
- 387 Gauthier, C., Solé, V.A., Signorato, R., Goulon, J., and Moguiline, E. (1999) The
388 ESRF beamline ID26: X-ray absorption on ultra dilute sample. *Journal of
389 Synchrotron Radiation*, **6**, 164-166.
- 390 Giorgetti, G., Marescotti, P., Cabella, R., and Lucchetti, G. (2001) Clay mineral
391 mixtures as alteration products in pillow basalts from the eastern flank of Juan
392 de Fuca Ridge: a TEM-AEM study. *Clay Minerals*, **36**, 75-91.
- 393 Giuli, G., Paris, E., Brigatti, M.F., Wu, Z., Mottana, A., Marcelli, A., and Cibin, G.
394 (2001) Experimental and theoretical XANES and EXAFS study of
395 tetraferriphlogopite. *European Journal of Mineralogy*, **13**, 1099-1108.
- 396 Giuli, G., Pratesi, G., Paris, E., and Cipriani, C. (2002) Fe local structure in tektites by
397 EXAFS and High resolution XANES spectroscopy. *Geochimica et
398 Cosmochimica Acta*, **66**, 4347-4353.
- 399 Giuli, G., Paris, E., Pratesi, G., Koeberl, C., and Cipriani, C. (2003) Iron oxidation
400 state in Fe-rich layer and silica matrix of Lybian Desert Glass: a high
401 resolution XANES study. *Meteoritics & Planetary Sciences*, **38**, 1181-1186.

- 402 Giuli, G., Eeckhout, S.G., Paris, E., Koeberl, C., and Pratesi, G. (2005) Iron oxidation
403 state in impact glass from the K/T boundary at Beloc, Haiti, by high-resolution
404 XANES spectroscopy. *Meteoritics & Planetary Science*, **40**, 1575-1580.
- 405 Giuli, G., Eeckhout, S.G., Koeberl, C., Pratesi, G., and Paris E. (2008a), Yellow
406 impact glass from the K/T boundary at Beloc (Haiti): XANES determination
407 of the Fe oxidation state and implications for formation conditions.
408 *Meteoritics & Planetary Science*, **43**, 981-986.
- 409 Giuli, G., Eeckhout, S.G., Cicconi, M.R., Koeberl, C., Glass, B.P., Pratesi, G., and
410 Paris, E. (2008b) North American microtektites are more oxidized compared
411 to tektites. Large Meteorite Impacts and Planetary Evolution IV,
412 Johannesburg, *Lunar and Planetary Institute* 1423, p. 88-89 (abstr.).
- 413 Giuli, G., Eeckhout, S.G., Cicconi, M.R., Koeberl, C., Pratesi, G., and Paris, E.
414 (2010a) Iron oxidation state and local structure in North American tektites. In
415 *Large Meteorite Impacts and Planetary Evolution IV* (W.U. Reimold and R.
416 Gibson eds.), Geological Society of America Special Paper **465**, 645-652.
- 417 Giuli, G., Pratesi, G., Eeckhout, S.G., Koeberl, C., and Paris, E. (2010b) Iron
418 reduction in silicate glass produced during the 1945 nuclear test at the trinity
419 site (Alamogordo, New Mexico, USA). In *Large Meteorite Impacts and*
420 *Planetary Evolution IV* (W.U. Reimold and R. Gibson eds.), Geological
421 Society of America Special Paper **465**, 653-662.
- 422 Giuli, G., Eeckhout, S.G., Cicconi, M.R., Koeberl, C., Glass, B.P., Pratesi, G.,
423 Cestelli-Guidi M., Marcelli A., Carroll, M.R., and Paris, E. (2010c) Tektites
424 and microtektites Fe oxidation state and water content. Proceedings of the 20th
425 General Meeting of the International Mineralogical Association. 21-27 August
426 2010, Budapest (H), *Acta Mineralogica Petrographica*, **6**, 777 (abstr.).

- 427 Giuli, G., Paris, E., Hess, K.U., Dingwell, D.B., Cicconi, M.R., Eckhout, S.G., Fehr,
428 K.T., and Valenti, P. (2011) XAS determination of the Fe local environment
429 and oxidation state in phonolite glasses and implications for the viscosity of
430 silicate melts. *American Mineralogist*, **96**, 631-636.
- 431 Giuli, G., Cicconi, M. R., Eeckhout, S. G., Paris, E., Pratesi, G., and Folco, L. (2012)
432 Fe Oxidation State in Microtektites from the Transantarctic Mountains. 43rd
433 Lunar and Planetary Science Conference, March 19–23, The Woodlands,
434 Texas. LPI Contribution No. 1659, id.1927.
- 435 Glass, B.P. (1967) Microtektites in deep-sea sediments. *Nature* **214**, 372-374.
- 436 Glass, B.P. (1968) Glassy objects (microtektites?) from deep-sea sediments near the
437 Ivory Coast. *Science New Series* **161**, n. 3844, 891-893.
- 438 Glass, B.P. (1972) Australasian microtektites in deep-sea sediments. In *Antarctic*
439 *Oceanology II: The Australian-New Zealand Sector, Antarctic Research*
440 *Series* (D.E. Hayes ed.) **19**, 335-348, American Geophysical Union.
- 441 Glass, B.P. (1989) North American tektite debris and impact ejecta from DSDP Site
442 612. *Meteoritics* **24**, 209-218.
- 443 Glass, B.P. (1990) Tektites and microtektites: key facts and inferences.
444 *Tectonophysics* **171**, 393-404.
- 445 Glass, B.P., Senftle, F.E., Muenow, D.W., Aggrey, K.E., and Thorpe, A.N. (1988)
446 Atomic bomb glass beads: tektite and microtektite analogs. In Proceedings,
447 Second International Conference on Natural Glasses, Prague, September 1987,
448 361-369
- 449 Glass, B.P. and Pizzuto, J.E. (1994) Geographic variation in Australasian microtektite
450 concentrations: Implications concerning the location and size of the source
451 crater. *Journal of Geophysical Research* **99**, n. E9, 19075-19081.

- 452 Glass, B.P., Koeberl, C., Blum, J.D., Senftle, J., Izett, G.A., Evans, B.J., Thorpe,
453 A.N., Povenmire, H., and Strange R.L. (1995) A Muong Nong –type Georgia
454 tektite. *Geochimica et Cosmochimica Acta*, **59**, 4071-4082.
- 455 Glass, B.P., Koeberl, C., Blum, J.D., and McHugh C.M.G. (1998) Upper Eocene
456 tektite and impact ejecta layer on the continental slope off New Jersey.
457 *Meteoritics & Planetary Science*. **33**, 229-241.
- 458 Glass, B.P., Huber, H., and Koeberl, C. (2004) Geochemistry of Cenozoic
459 microtektites and clinopyroxene-bearing spherules. *Geochimica et*
460 *Cosmochimica Acta*, **68**, 3971-4006.
- 461 Jackson, W.E., Farges, F., Yeager, M., Mabrouk, P.A., Rossano, S., Waychunas,
462 G.A., Solomon, E.I., and Brown, G.E. JR. (2005) Multi-spectroscopic study of
463 Fe(II) in silicate glasses: Implications for the coordination environment of
464 Fe(II) in silicate melts. *Geochimica et Cosmochimica Acta*, **69**, 4315–4332
- 465 Koeberl, C. (1986) Geochemistry of tektites and impact glasses: Annual Reviews of
466 Earth and Planetary Science, v. 14, p. 323-350.
- 467 Koeberl, C. (1994) Tektite origin by hypervelocity asteroidal or cometary impact:
468 Target rocks, source craters, and mechanisms. In: Large Meteorite Impacts
469 and Planetary Evolution (Ed. B.O. Dressler, R.A.F. Grieve, and V.L.
470 Sharpton), Boulder, Geological Society of America Special Paper 293, p. 133-
471 152.
- 472 Krause, M.O. and Oliver J.H. (1979) Natural widths of atomic K and L levels, K
473 alpha X-ray lines and several KLL auger lines. *Journal of Physical and*
474 *Chemical Reference Data*, **8**, 329-338.
- 475 Montanari, A. and Koeberl C. (2000) Impact stratigraphy. *Lecture Notes in Earth*
476 *Sciences* **93**, Springer Verlag, Heidelberg-Berlin, 364 p.

- 477 Rossano, S., Balan, E., Morin, G., Bauer, J.P., Calas, G., and Brouder C. (1999) ^{57}Fe
478 Mössbauer spectroscopy of tektites. *Physics and Chemistry of Minerals*, **26**,
479 530-538.
- 480 Senftle, F.E., Thorpe, A.N., and Sullivan S. (1969) Magnetic properties of
481 microtektites. *Journal of Geophysical Research*, **74**, 6825-6833.
- 482 Solé, A.V., Gauthier, C., Goulon, J., and Natali, F. (1999) Undulator QEXAFS at the
483 ESRF beamline ID26. *Journal of Synchrotron Radiation*, **6**, 174-175.
- 484 Weigel, C., Cormier, L., Galois, L., Calas, G., Bowron, D., and Beuneu, B. (2006)
485 Determination of Fe^{3+} sites in a $\text{NaFeSi}_2\text{O}_6$ glass by neutron diffraction with
486 isotopic substitution coupled with numerical simulation. *Applied Physics*
487 *Letters*, **89**, 141911
- 488 Weigel, C., Cormier, L., Calas, G., Galois, L., and Bowron, D.T. (2008) Nature and
489 distribution of iron sites in a sodium silicate glass investigated by neutron
490 diffraction and EPSR simulation. *Journal of Non-Crystalline Solids*, **354**,
491 5378-5385.
- 492 Wilke, M., Farges, F., Petit, P.E., Brown, G.E., and Martin, F. (2001) Oxidation state
493 and coordination of Fe in minerals: an Fe K-XANES spectroscopic study.
494 *American Mineralogist*, **86**, 714-730.
- 495 Wilke, M., Partzsch, G.M., Bernhardt, R., and Lattard D. (2004) Determination of the
496 iron oxidation state in basaltic glasses using XANES at the K-edge. *Chemical*
497 *Geology*, **213**, 71-87.
- 498 Wilke, M., Schmidt, C., Farges, F., Malavergne, V., Gautron, L., Simionovici, A.,
499 Hahn, M., and Petit, P-E (2006) Structural environment of iron in hydrous
500 aluminosilicate glass and melt-evidence from X-ray absorption spectroscopy.
501 *Chemical Geology*, **229**, 144-161
502

503 **Figure captions**

504

505 Fig. 1 Total alkalis versus silica contents of the analyzed North American
506 microtektites. For source of compositional data see Table 1. The open rectangle
507 represents the range in the silica and alkali contents for North American tektites as
508 reported by Glass et al. (1995, 1998) and Montanari and Koeberl (2000). Each sample
509 group was given the designation NA plus the sample name (3 digit number) as
510 reported in Glass et al. (2004) and the collection site.

511

512 Fig. 2: Experimental Fe K-edge XANES spectra of microtektites: a) Ivory
513 Coast; b) Australasian; c) North American (DSDP 612); d) North American (DSDP
514 149); e) North American (Barbados). Pre-edge peak is labeled “P”. The spectra labels
515 are the same as sample names in Table 1. The first three digits refers to the disc
516 number the microtektites were mounted on and the number after the hyphen refers to
517 the number of the microtektite on that disc.

518

519 Fig. 3: Background subtracted pre-edge peaks: a) Ivory Coast; b) Australasian;
520 c) North American (DSDP Site 612); d) North American (DSDP Site 149) ; e) North
521 American (Barbados). Labels as in Fig. 2.

522

523 Fig. 4: Pre-edge peak integrated area versus centroid energy of : a) Ivory Coast
524 and Australasian microtektites; b) North American microtektites. Symbols as in Fig.
525 1. The 0 on the x axis refers to the edge energy of metallic iron (7112.0 eV).

526

527 Fig. 5: Alkali content (oxide wt %) as a function of the fraction of trivalent Fe
528 in the studied microtektites. The amount of both Na₂O and K₂O does not show any
529 significant decrease as would be expected in case of sea water alteration.

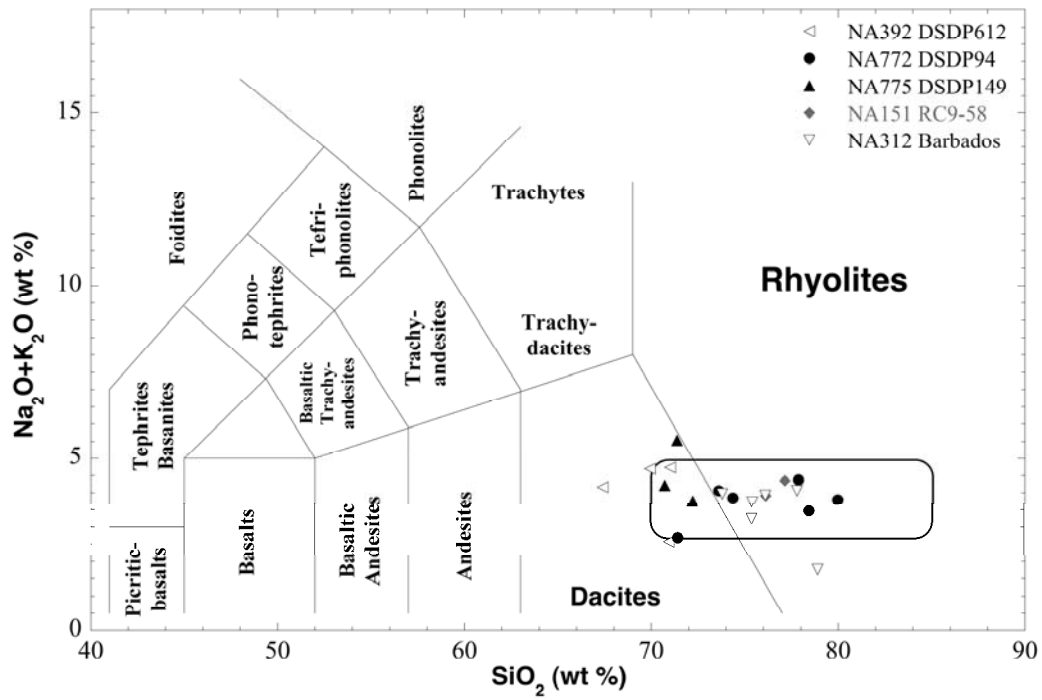
530

531 Fig. 6: Trivalent Fe fraction of the NA microtektites as a function of collection
532 site distance from the source crater (symbols as in Fig 4b). A marked increase of the
533 trivalent Fe at increasing distance from the crater is evident.

534

535

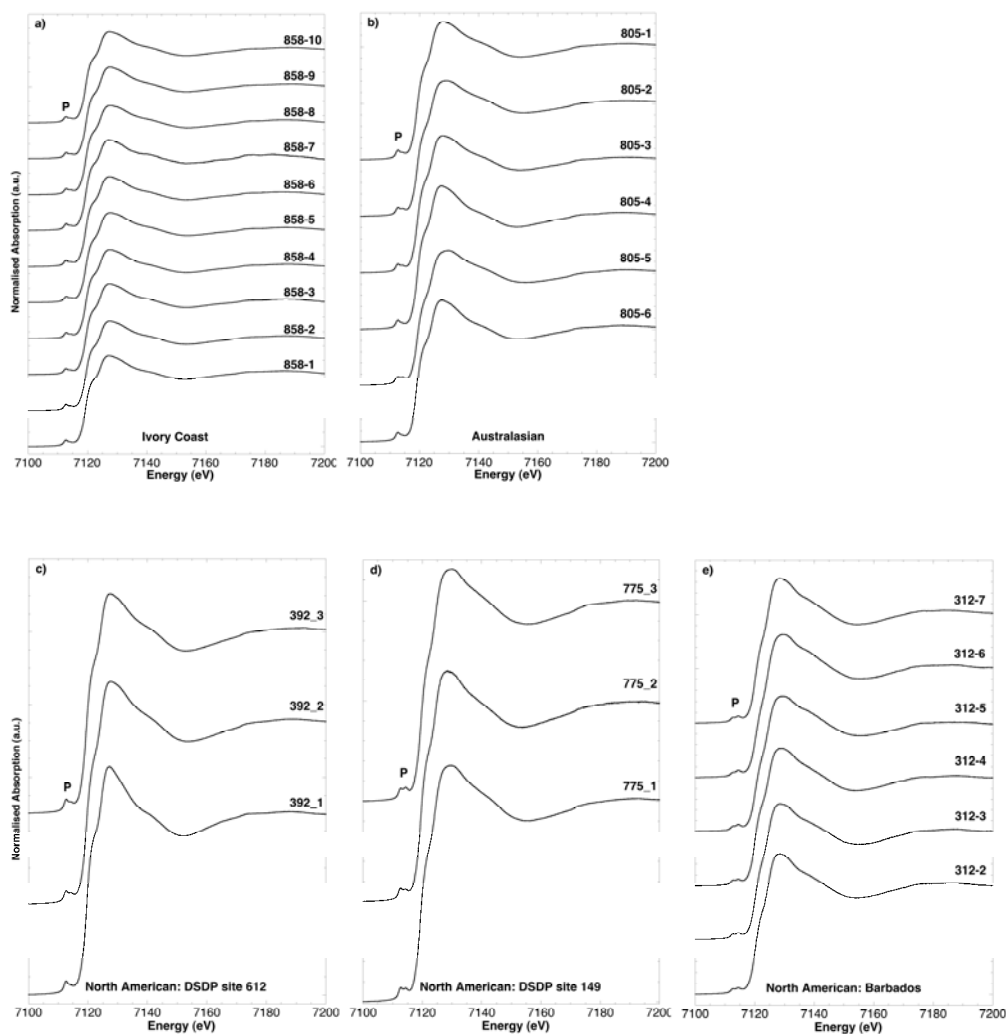
536 Fig.1



537

538

539 Fig. 2

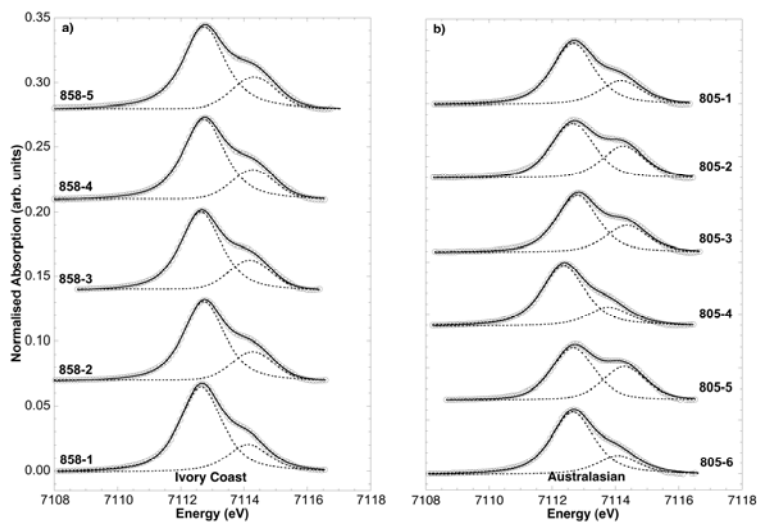


540

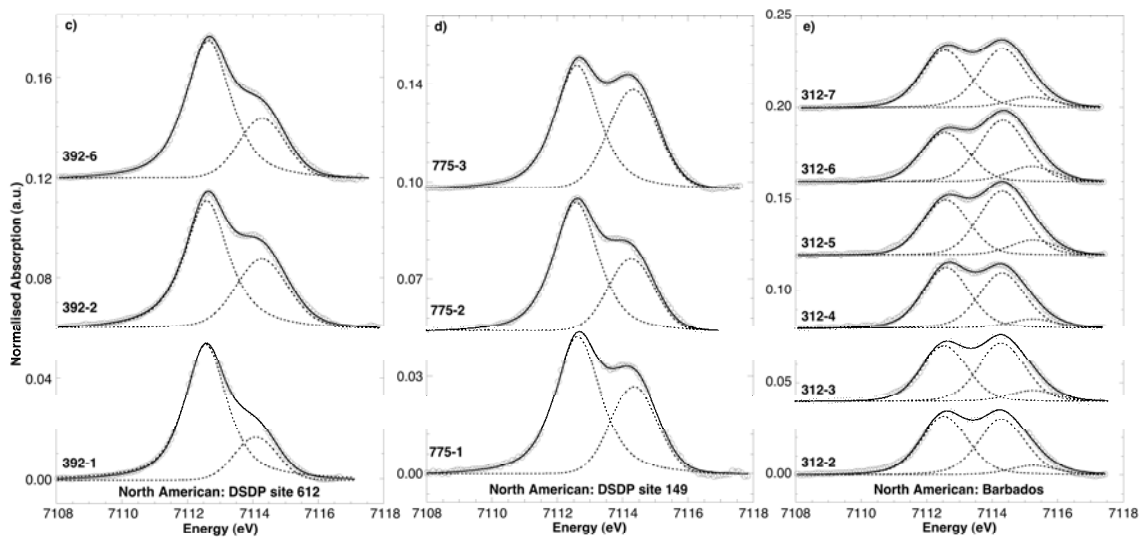
541

542

543 Fig. 3



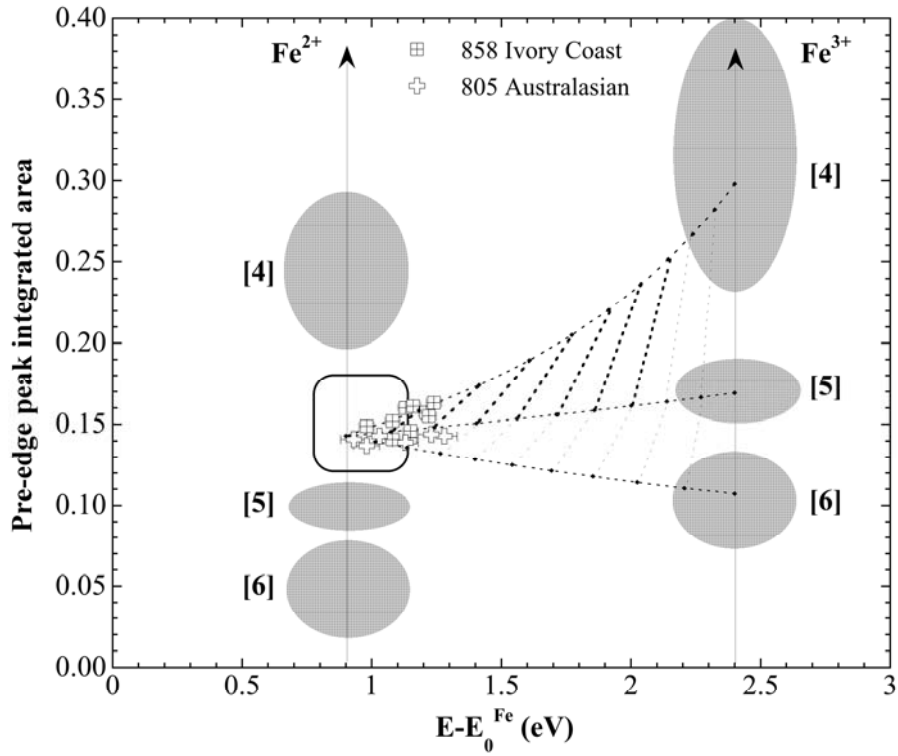
544



545

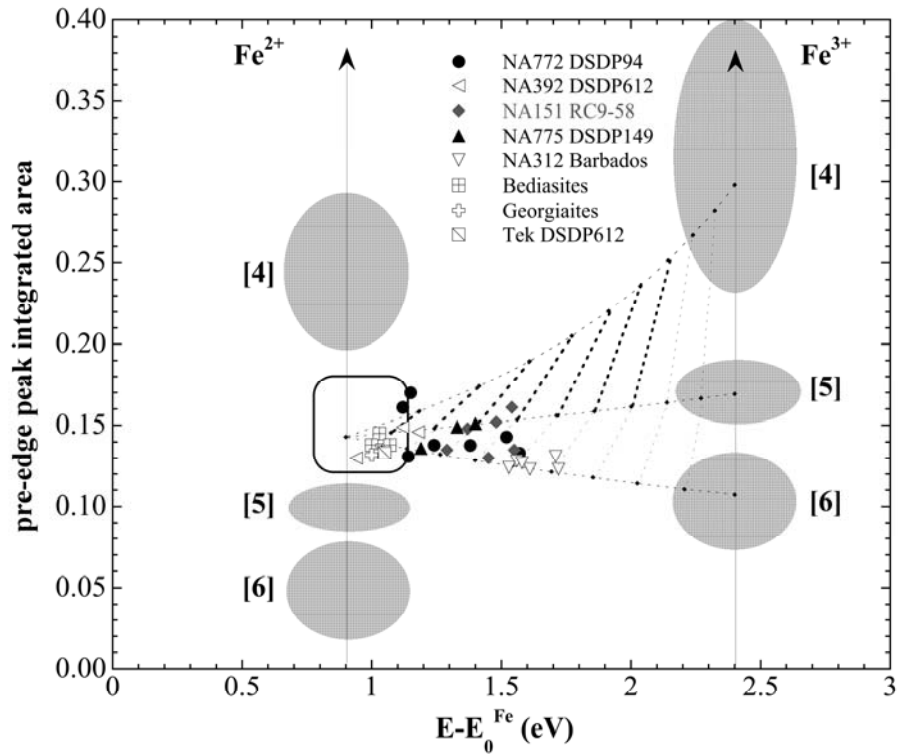
546

547 Fig. 4a



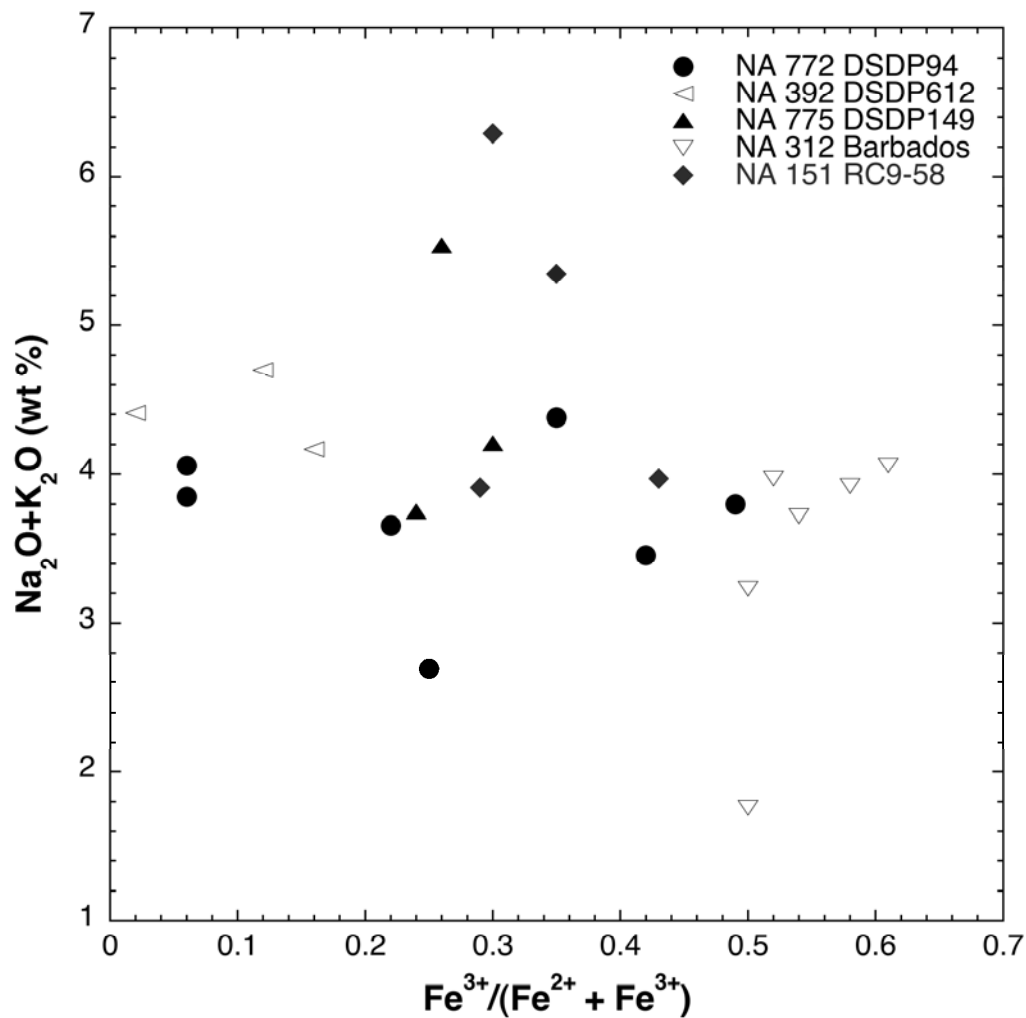
548

549 Fig. 4b



550

551 Fig. 5

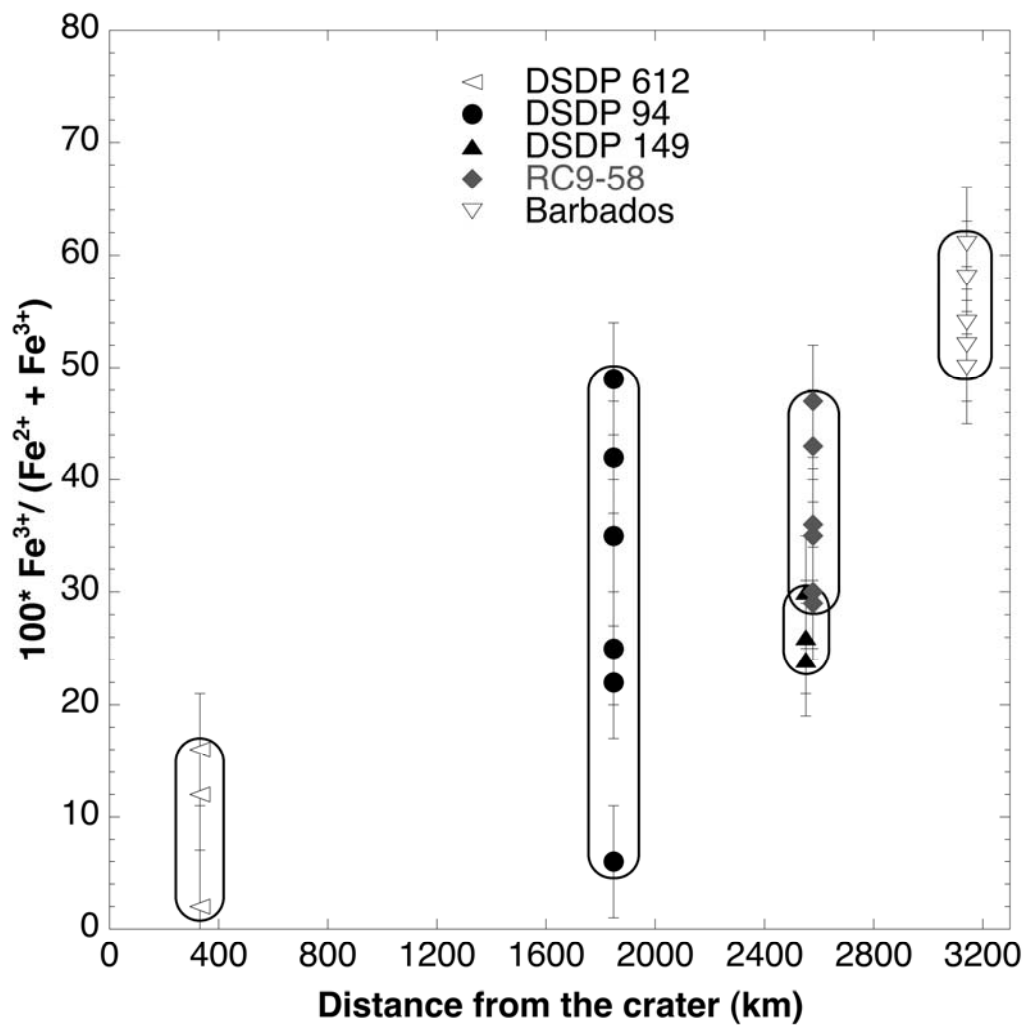


552

553

554

555 Fig.6



556

Table 1. Composition of the studied microtektites in wt% oxides.

Sample	core	SiO ₂	Al ₂ O ₃	Cr ₂ O ₃	FeO	CaO	MgO	K ₂ O	Na ₂ O	TiO ₂	total	Source [†]
Australasian microtektites												
805-1	ODP769A	64.72	16.21	0.03	5.39	3.9	7.77	0.48	0.62	0.87	99.99	1
805-2	ODP769A	70.09	13.54	0.01	5.74	2.68	3.02	2.77	1.37	0.75	99.97	1
805-3	ODP769A	66.84	16.71	0.01	5.65	2.72	2.62	3.21	1.39	0.83	99.98	1
805-4	RC12-331	56.05	20.66	0.05	4.5	5.72	11.34	0.13	0.43	1.17	100.05	1
805-5	RC14-46	67.17	14.94	0.01	5.97	3.68	3.07	2.79	1.59	0.8	100.02	1
805-6	RC14-46	69.25	12.48	0.04	6.77	3.29	4.17	2.22	1.04	0.69	99.95	1
Ivory Coast microtektites												
858-1	K9-56	63.68	17.62	0.05	7.44	2.09	6.15	1.03	1.67	0.57	100.30	1
858-2	K9-56	69.30	15.82	0.02	5.67	1.48	3.25	1.89	2.10	0.47	100.00	1
858-3	K9-56	67.35	17.15	0.01	6.39	1.56	3.13	1.90	1.98	0.54	100.01	1
858-4	K9-56	67.33	16.50	0.02	6.48	1.63	3.86	1.65	1.96	0.58	100.01	1
858-5	K9-56	67.12	15.97	0.02	6.53	1.88	4.20	1.82	1.96	0.50	100.00	1
858-6	K9-56	67.38	16.89	0.02	6.31	1.54	3.31	1.96	2.09	0.52	100.02	1
858-7	K9-56	68.11	17.02	0.02	6.67	1.05	2.91	2.03	1.60	0.54	99.95	1
858-8	K9-56	67.86	16.23	0.02	6.34	1.81	3.84	1.54	1.80	0.53	99.97	1
858-9	K9-56	68.00	16.90	0.02	6.55	1.14	3.15	1.95	1.72	0.58	100.01	1
858-10	K9-56	67.59	16.73	0.02	6.19	1.54	3.37	1.96	2.03	0.54	99.97	1
North American microtektites												
772-1	DSDP94	71.44	17.62	0.05	5.98	0.43	0.95	1.64	1.05	0.90	100.06	1
772-2	DSDP94	77.87	11.66	0.02	3.09	1.29	1.10	3.16	1.22	0.60	100.01	1
772-3	DSDP94	74.36	13.82	0.03	3.51	2.01	1.68	2.60	1.25	0.74	100.00	1
772-4	DSDP94	78.47	11.78	0.02	3.12	1.30	1.23	2.52	0.94	0.60	99.98	1
772-5	DSDP94	73.60	13.87	0.05	4.17	1.78	1.76	2.74	1.32	0.76	100.05	1
772-6	DSDP94	81.51	10.82	0.01	2.28	0.45	0.80	2.74	0.92	0.46	99.99	1
772-7	DSDP94	79.97	11.03	0.02	2.78	0.94	0.96	3.02	0.78	0.51	100.01	1
392-1	DSDP612	71.01	16.10	n.d.	4.16	1.61	1.23	1.40	3.01	0.85	99.37	3
392-2	DSDP612	67.38	15.50	n.d.	5.43	2.63	3.49	1.52	2.65	0.75	99.35	2
392-6	DSDP612	69.94	15.10	n.d.	4.33	2.11	2.60	1.51	3.19	0.65	99.43	2
151-91a	RC9-58	75.19	12.73	n.d.	3.04	1.52	1.30	4.07	1.28	0.46	99.59	3
151-93b	RC9-58	67.52	16.06	n.d.	5.51	1.42	1.69	4.84	1.45	1.07	99.56	3

151-94a	RC9-58	79.63	11.31	n.d.	2.59	0.52	1.00	2.95	1.02	0.53	99.55	3
151-102a	RC9-58	76.12	13.37	n.d.	3.62	0.97	1.00	2.99	0.92	0.66	99.65	3
775-1	DSDP149	71.38	14.57	n.d.	4.29	1.55	1.95	4.30	1.24	0.73	100.01	1
775-2	DSDP149	72.22	15.63	n.d.	4.90	1.15	1.48	2.86	0.89	0.85	99.98	1
775-3	DSDP149	70.72	16.30	n.d.	4.68	1.56	1.68	3.20	1.01	0.84	99.99	1
312-2	Barbados	75.40	13.20	n.d.	4.95	0.76	1.00	2.31	0.92	0.60	99.14	4
312-3	Barbados	75.40	13.60	n.d.	3.58	1.26	0.97	2.70	1.02	0.65	99.18	4
312-4	Barbados	78.90	13.70	n.d.	1.56	1.88	0.70	1.55	0.21	0.61	99.11	4
312-5	Barbados	77.80	12.40	n.d.	2.78	1.03	0.64	3.08	0.98	0.52	99.23	4
312-6	Barbados	76.10	13.30	n.d.	3.75	0.77	0.69	2.33	1.59	0.69	99.22	4
312-7	Barbados	73.80	14.20	n.d.	4.29	1.43	1.17	2.65	1.32	0.68	99.54	4

[†]1 = Glass et al. (2004); 2 = Glass (1989); 3 = this study; 4 = Burns (1985).

Table 2. Pre-edge peak features in the samples studied.

Sample name	Centroid (eV) ^a	Integrated intensity	Fit agreement index (%)	Fe ³⁺ /(Fe ²⁺ +Fe ³⁺)
Ivory Coast microtektites				
858-1	7112.98	0.149	99.97	0.03
858-2	7113.15	0.142	99.95	0.17
858-3	7113.08	0.141	99.96	0.12
858-4	7113.15	0.146	99.97	0.15
858-5	7113.21	0.157	99.97	0.12
858-6	7113.13	0.160	99.97	0.08
858-7	7113.16	0.161	99.97	0.09
858-8	7113.24	0.163	99.96	0.13
858-9	7113.22	0.155	99.97	0.15
858-10	7113.08	0.152	99.97	0.06
Australasian microtektites				
805-1	7112.93	0.141	99.92	0.02
805-2	7113.28	0.143	99.98	0.22
805-3	7112.98	0.137	99.96	0.04
805-4	7113.13	0.139	99.95	0.13
805-5	7113.23	0.144	99.92	0.19
805-6	7113.03	0.143	99.92	0.07
North American microtektites				
392-1	7112.94	0.130	99.98	0.02
392-2	7113.18	0.146	99.94	0.16
392-6	7113.12	0.149	99.95	0.12
775-1	7113.33	0.149	99.87	0.26
775-2	7113.19	0.136	99.94	0.24
775-3	7113.40	0.151	99.94	0.30
312-2	7113.56	0.128	99.87	0.50
312-3	7113.61	0.123	99.90	0.54
312-4	7113.53	0.124	99.89	0.50
312-5	7113.71	0.131	99.91	0.61
312-6	7113.72	0.123	99.92	0.58
312-7	7113.58	0.127	99.92	0.52
772-1	7113.24	0.138	99.96	0.25
772-2	7113.38	0.138	99.86	0.35
772-3	7113.15	0.170	99.94	0.06
772-4	7113.52	0.143	99.87	0.42
772-5	7113.12	0.161	99.92	0.06
772-6	7113.14	0.131	99.94	0.22
772-7	7113.57	0.133	99.85	0.49
151-91a	7113.48	0.152	99.93	0.35
151-93a	7113.54	0.161	99.95	0.36
151-93b	7113.29	0.135	99.95	0.30
151-94a	7113.45	0.130	99.93	0.43
151-101b	7113.55	0.135	99.92	0.47
151-102a	7113.37	0.148	99.96	0.29

^a The energy has been calibrated by setting the Edge energy of metallic Fe at 7112.0 eV